Journal of Hazardous Materials 382 (2020) 121028

Contents lists available at ScienceDirect

Journal of Hazardous Materials

journal homepage: www.elsevier.com/locate/jhazmat

The influence of highly dispersed Cu_2O-anchored MoS_2 hybrids on reducing smoke toxicity and fire hazards for rigid polyurethane foam

Yao Yuan[a,b,1], Wei Wang[a,1], Yongqian Shi[c], Lei Song[a], Chao Ma[a,*], Yuan Hu[a,*]

[a] *State Key Laboratory of Fire Science, University of Science and Technology of China, Hefei 230026, PR China*

[b] *Fujian Provincial Key Laboratory of Functional Materials and Applications, School of Materials Science and Engineering, Xiamen University of Technology, Xiamen 361024, PR China*

[c] *College of Environment and Resources, Fuzhou University, Fuzhou 350002, PR China*

GRAPHICAL ABSTRACT

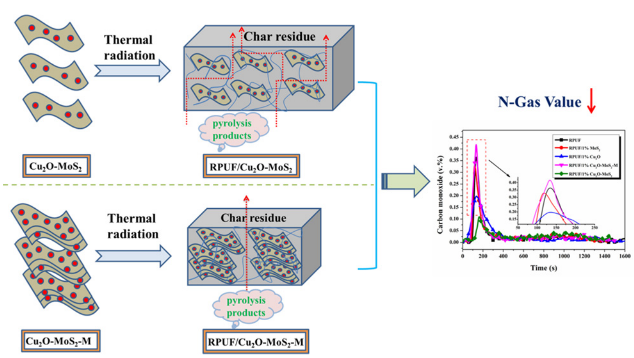

ARTICLE INFO

Editor: Danmeng Shuai

Keywords:
Toxic gases
Toxicity suppression
Cu_2O-MoS_2hybrids
Rigid polyurethane foam
N-Gas model

ABSTRACT

The extensive utilization of rigid polyurethane foam (RPUF) as construction insulation material has brought two main troubles to our society: fire risks and toxic hazards. To reduce the fire hazards of RPUF, a layered MoS_2 decorated with Cu_2O nanoparticles was creativity obtained by hydrothermal technology and facile wet chemical treatment for reducing the toxic product formations of polyurethane nanocomposites during combustion. Due to the low weight ratio of Cu_2O attached onto MoS_2, the resulting Cu_2O-MoS_2 hybrid effectively prevented the MoS_2 nanosheets from restacking. However, the Cu_2O-MoS_2-M hybrid was produced by increasing content of Cu_2O, which has the characteristic stacked layer structure of MoS_2. Reduced harmful organic volatiles and the toxic gases (e.g. a respective decrease of ca. 28% and 53% for CO and NO_x products) were obtained because of synergistic effect between the physical adsorption of MoS_2 and catalysis action of Cu_2O. Notably, the addition of Cu_2O-MoS_2 hybrids led to high char formation of the RPUF nanocomposite, indicating the effectively catalytic carbonization property. In addition, the N-Gas model for predicting fire smoke toxicity was developed and demonstrated. Furthermore, the research offers direct proofs of the negative influence of the stacked MoS_2 on reducing the smoke toxicity for RPUF nanocomposites.

* Corresponding authors.
E-mail addresses: mcsky@ustc.edu.cn (C. Ma), yuanhu@ustc.edu.cn (Y. Hu).
[1] These authors contributed equally to this work.

https://doi.org/10.1016/j.jhazmat.2019.121028
Received 10 February 2019; Received in revised form 31 July 2019; Accepted 15 August 2019
Available online 15 August 2019
0304-3894/

1. Introduction

Polyurethane (PU) is a significant member of polymers that is widely applied in many fields such as building insulation, household items, and automotive parts. Among PU materials, rigid polyurethane foam (RPUF), one of the most important commercial products, has been applied in household equipment and building material by reason of its gorgeous mechanical behavior and heating insulation property (Santos et al., 2017; Kacperski and Spychaj, 1999; Pauzi et al., 2014). Nevertheless, once combustion, RPUF will produce extreme amounts of heat because of its the cellular structure (Chattopadhyay and Webster, 2009; Zhang et al., 2014), generating toxic smoke and poisonous gases (Zhang et al., 2016). These deleterious products can bring fire disaster and increased the death toll (Wang et al., 2014a; Levchik and Weil, 2005; Carty and White, 1994; Ling et al., 2015). Consequently, generous investigations and efforts have been made to reduce the generation of smoke toxicity suppression which has great influence on the human society.

With the increasing demand for reduction of toxic hazards, intensive attention should be drawn to the development of catalysts for reducing poisonous gases (Yu et al., 2016). Generally, the deleterious gaseous agents composes by carbon monoxide (CO), nitrogen oxide (NO_x), hydrogen cyanide (HCN) and harmful smoke (Ling et al., 2015), in the process of combustion and degradation for RPUF. Normally, metal oxide catalysts have been applied to reduce the exhaust gases of internal combustion engines (Sun et al., 2010; White et al., 2006; Kröcher and Elsener, 2009; Moreno et al., 2014; Shi et al., 2017). Transition metal oxide nanoparticles have received much attention from researchers which play an important role in carbonization and detoxification of the deleterious products. Among various transition metal oxides catalysts, Cu_2O and its derivatives with high activity and stability have been investigated as highly-efficient catalysts for the treatments of CO, NO_x, HCN and organic compounds (Zhao et al., 2006; Sun et al., 2014), which render Cu_2O a promising suppressant for toxic gaseous products. Tu and Wang (1996) found that smoke emission of polyvinyl chloride (PVC) can be controlled by Cu_2O resulting from its charring effect and reductive-coupling in the condensed phase. White et al. (2006) confirmed that Cu_2O exhibits predominant activity toward CO oxidation in $CO/N_2/O_2$ mixtures, and more than 99.5% transformation of CO to CO_2 has been realized.

Recently, MoS_2 has received considerable attention, which possesses a layered structure by van der Waals forces similar to graphene, because of its excellent performances such as thermal and chemical stability, and catalytic potential in the field of environmental and industrial catalysis research (Dinter et al., 2009; Breysse et al., 2008; Yu et al., 2015). More recently, MoS_2 nanosheets have been applied into polymer composites, which enormously improved their physical and chemical properties (Wang et al., 2017). Deng et al. found that water-dispersed noble metal nanocrystal modified MoS_2 nanosheets exhibit improved electrochemical catalytic activity compared to the individual property (Lee et al., 2010). Nevertheless, exfoliated MoS_2 nanosheets actually have a trend toward agglomeration and even restacking due to the strong van der Waals force that reduces their compatibility in polymers. It is reported that only the uniform dispersion of MoS_2 nanosheets can achieve the improvement of fire safety (Yuwen et al., 2014). Notably, Feng et al. found that the restacking of the two-dimensional MoS_2 nanosheets could be efficiently prevented by the densely anchored nanoparticulates, that was beneficial for the homogeneous dispersion of MoS_2 nanosheets with polymers (Feng et al., 2014). Nonetheless, MoS_2 nanosheets on boosting the activity of Cu_2O on the MoS_2 surface for catalytic oxidation of CO production of RPUF nanocomposites are scarcely reported. Thus, it is reasonable to expect that the Cu_2O loaded on MoS_2 is the critical point lies in achieving high dispersion of MoS_2 nanosheets and thus restraining the fire hazards of RPUF.

To provide and guide the primary and immediate toxicity studies in a fire, the N-Gas model for predicting toxic hazard has been proposed by NIST (the USA National Institute of Standards and Technology) for many years (Levin, 1996). This method makes the calculation of the toxic potency of fire smoke components available on the basis of the interaction of acute toxicity among the main components, oxygen depletion (ΔO_2), carbon monoxide (CO), carbon dioxide (CO_2), hydrogen cyanide (HCN) and nitrogen oxide (NO_x), hydrogen chloride (HCl), hydrogen bromide (HBr) (Levin, 1996). Essentially, the method of calculating toxic potency is based on the ratios of gaseous concentrations. On account of the experience formerly, the following 7-gas N-Gas model was presented:

$$\begin{aligned} \text{N}-\ \text{Gas Value} = & \frac{m[CO]}{[CO_2]-b} + \frac{21-[O_2]}{21-LC_{50}(O_2)} \\ & + \left(\frac{[HCN]}{LC_{50}(HCN)} \times \frac{0.4[NO_2]}{LC_{50}(NO_2)}\right) + 0.4\left(\frac{[NO_2]}{LC_{50}(NO_2)}\right) \\ & + \frac{[HCl]}{LC_{50}(HCl)} + \frac{[HBr]}{LC_{50}(HBr)} \end{aligned} \tag{1}$$

Where the LC50 (ppm) values are reference concentrations (RFC) of main gas components, which lead to death when inhaled for a specified time, typically 30 min. The terms “m” and “b” in equation connect with the elevated ventilation rate ascribed to the CO_2 concentration. For researches when the CO_2 concentration surpasses 5%, ‘m’ and ‘b’ equal 23 and -38600, respectively, whereas the ‘m’ and ‘b’ are -18 and 122,000 if the CO_2 concentration is 5% or less.

Herein, we reported a facile wet chemical route for the preparation of Cu_2O-MoS_2 hybrids with different loadings of tiny Cu_2O nanoparticles onto the surface of MoS_2 nanosheets by a facile wet chemical route. The optimal proportion of Cu_2O and MoS_2 was 1:1 which contributed to preventing restacking of MoS2 nanosheets. However, a large numbers of restacked MoS_2 nanosheets were identified obviously with high weight ratio of Cu_2O to MoS_2, which was labeled as Cu_2O-MoS_2-M. In particular, Cu_2O-MoS_2 hybrid boosting the activity of toxicity suppression in RPUF has been clarified by comparison to Cu_2O-MoS_2-M hybrid. More importantly, the Cu_2O-MoS_2 hybrid provided the incremental quantity of catalytic active-sites afforded by the absence of stacked MoS_2 layers (Yang et al., 2015). Our research offers tangible proofs of the passive effects of the stacked MoS_2 nanosheets of Cu_2O-MoS_2-M hybrids on improving the ability of toxicity suppression and highlighting the importance of more rational use of Cu_2O loaded on MoS_2 for reducing the fire hazards of RPUF by means of N-Gas values which were generated and calculated by N-Gas model using the concentrations of fire effluents.

2. Experimental section

2.1. Raw materials

Molybdenum disulfide (MoS_2, AP), n-hexane (AP), copper acetate monohydrate ($Cu(CH_3COO)_2 \cdot H_2O$, AP), poly(N-vinylpyrrolidone) (PVP), hydrazine hydrate (85% aq.), absolute ethanol (C_2H_5OH) and triethanolamine (TEOA) were all obtained from Sinopharm Chemical Reagent Co., Ltd. N-Butyl lithium was supplied by Aladdin Industrial Corporation. Polyol LY-4110, polyaryl polymethylene isocyanate, dibutyltin dilaurate (LC), triethylenediamine (A33), and silicone surfactant were graciously provided by Jiangsu Luyuan New Materials Co., Ltd, China.

2.2. Preparation of LixMoS$_2$

LixMoS$_2$ was obtained using the hydrothermal route by adding 36 mL of a 0.5 M solution in hexane of n-butyl lithium to 1.0 g of raw MoS_2 in a teflon autoclave. Subsequently, the autoclave was heated at 100 °C for 4 h, followed by cooling naturally. The resulting products were rinsed with anhydrous hexane by filtration, followed by drying at 55 °C for 6 h in a vacuum chamber.

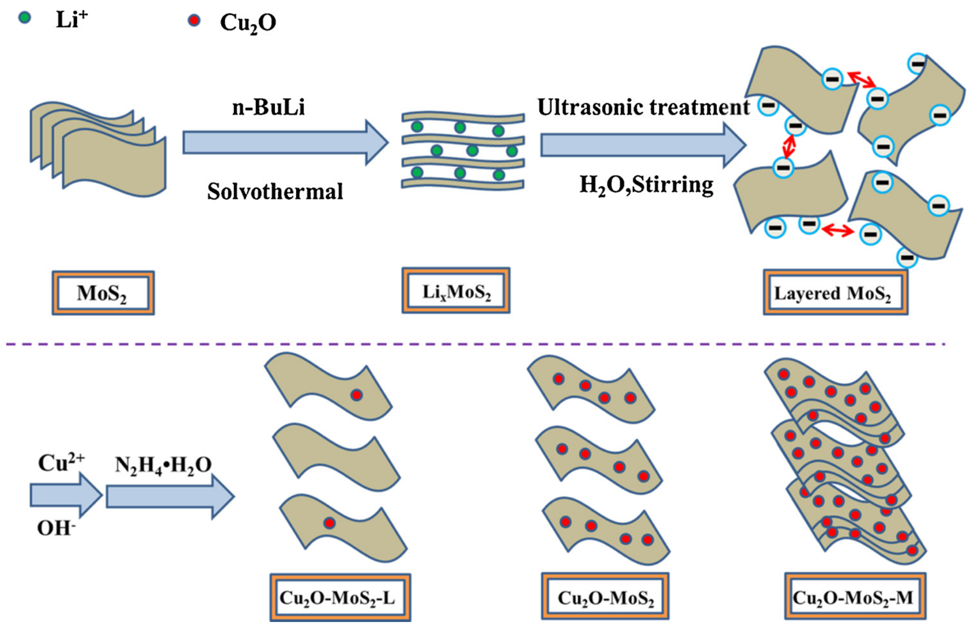

Scheme 1. Schematic presentation of the formation mechanism of the Cu_2O-MoS_2 hybrids.

Table 1
The formulae of pristine RPUF, RPUF/MoS_2, RPUF/Cu_2O-MoS_2 and RPUF/Cu_2O-MoS_2-M composites.

Samples	RPUF-1	RPUF-2	RPUF-3	RPUF-4	RPUF-5
LY4110 (g)	100	100	100	100	100
A33 (g)	1	1	1	1	1
LC (g)	0.5	0.5	0.5	0.5	0.5
Water (g)	1	1	1	1	1
Si-Oil (g)	2	2	2	2	2
TEA (g)	3	3	3	3	3
MoS_2	0	2.45	0	0	0
Cu_2O-MoS_2	0	0	0	2.45	0
Cu_2O-MoS_2-M	0	0	0	0	2.45
PM-200 (g)	135	135	135	135	135

2.3. Preparation of Cu_2O-MoS_2 hybrids

The acquisition of ultrathin MoS_2 was based on a one-step ultrasonic and hydrolysis route of Li$x$$MoS_2$ into deionized water at ambient conditions and Cu_2O-MoS_2 hybrids obtained by the very facile wet chemical treatment is shown in Scheme 1. In the first step, 0.2 g of Li$x$$MoS_2$ was added into 500 mL of deionized water and ultrasonic agitated at ambient temperature for 5 h to acquire a colloidal suspension. After that, $Cu(CH_3COO)_2{\cdot}H_2O$ (0.2 g) was mixed with 0.2 g of PVP aqueous solution (10 mL) and then added in the above suspension with 24 h continuous agitation at room temperature. Subsequently, 0.03 g of hydrazine hydrate ($N_2H_4{\cdot}H_2O$) was dropped with constant agitation and ultrasonication. 20 min later, the black deposit was centrifuged and washed several times, dried in a chamber and stored under nitrogen. Other samples with different mass (i.e. 0.1 g and 0.4 g) from Cu $(CH_3COO)_2{\cdot}H_2O$ were prepared using the similar procedure, which are labeled as Cu_2O-MoS_2, Cu_2O-MoS_2-L and Cu_2O-MoS_2-M.

2.4. RPUF/Cu_2O-MoS_2 composites fabrication

In a typical procedure, 0.78 g of Cu_2O-MoS_2 hybrid was added into 45 g of PAPI with agitation and ultrasonication to obtain a uniform suspension at ambient condition. Afterwards, the RPUF composite was prepared by a one-pot and free-rise treatment according to our previous work (Yuan et al., 2016). Briefly, all the basic material except above suspension was agitated vigorously in a beaker. Subsequently, the two mixtures were adequately intermixed for 12 s and then quickly transferred into a mould. In addition, Table 1 lists sample descriptions. Finally, the RPUF/Cu_2O-MoS_2 composite was allowed to cure for 28 h. In addition, the same procedure was followed to prepare pristine RPUF, RPUF/Cu_2O-MoS_2, RPUF/Cu_2O-MoS_2 and RPUF/Cu_2O-MoS_2-M (-L) composites, while the nanofiller loading in all the samples was maintained at 1 wt%.

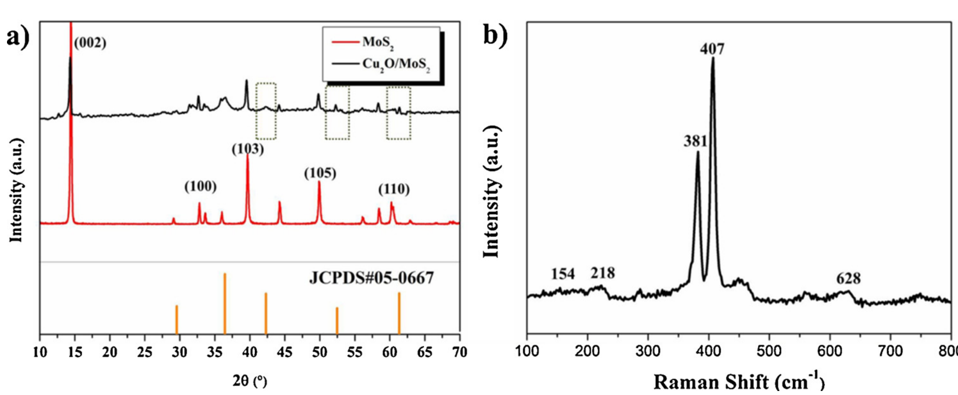

Fig. 1. XRD patterns of the MoS_2 and Cu_2O-MoS_2 hybrid (a) and Raman spectrum of Cu_2O-MoS_2 hybrid (b).

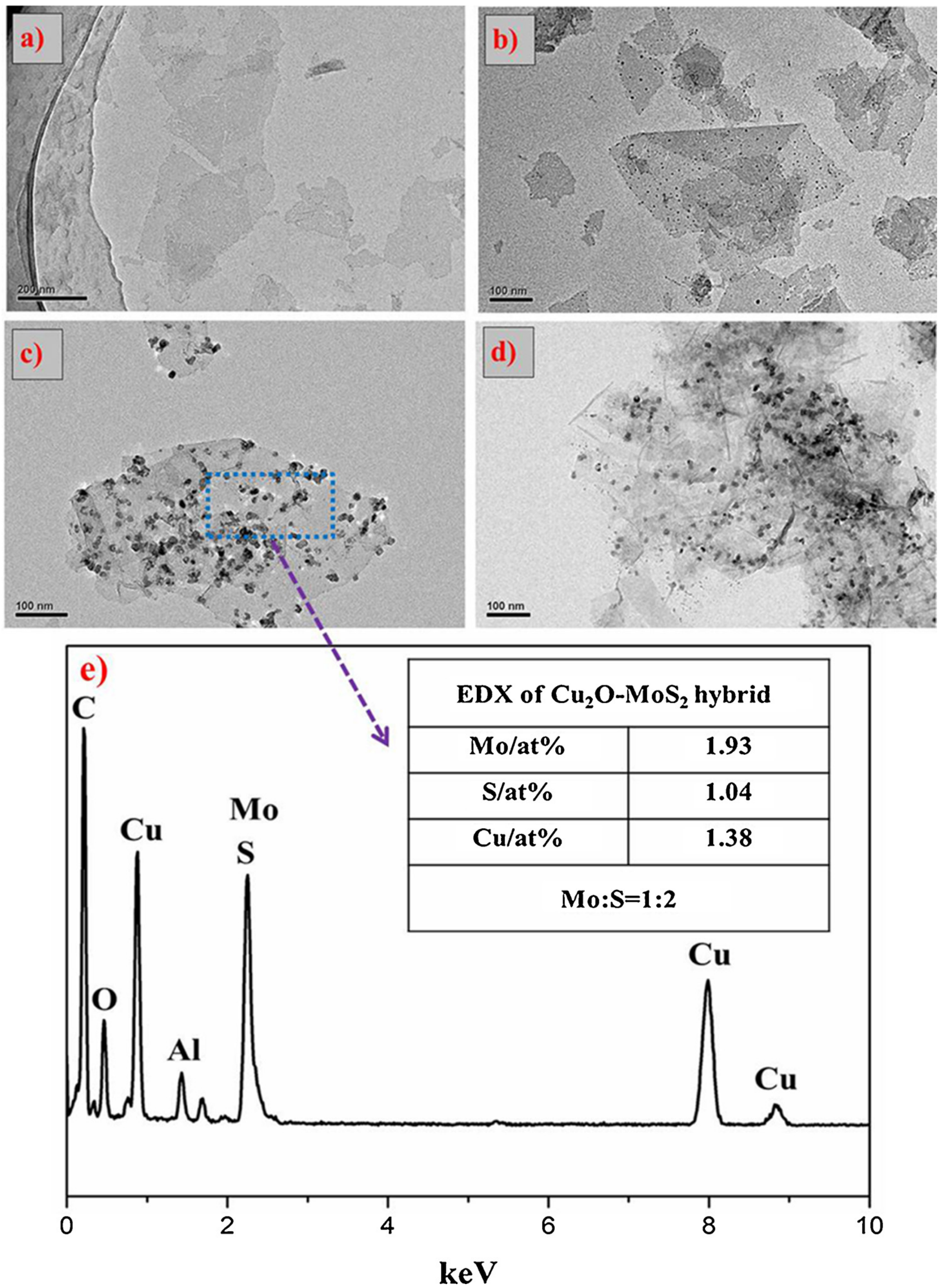

Fig. 2. TEM of the MoS_2 and Cu_2O-MoS_2 hybrids images: MoS_2 nanosheets (a), Cu_2O-MoS_2-L hybrid (b), Cu_2O-MoS_2 hybrid (c), Cu_2O-MoS_2-M hybrid (d) and EDX spectrum of Cu_2O-MoS_2 hybrid (e).

2.5. Characterization

Crystal-phase properties of the samples were studied by a powder X-ray diffractometer (Japan Rigaku D Max-Ra) using a rotating anode X-ray diffractometer accompanied with a Ni filtered Cu-Ka tube (λ = 1.54178 Å) in the 2θ range from 10° to 70° with a sweep speed of 4 min^{-1}.

Element composition and morphology of Cu_2O-MoS_2 hybrid were observed by transmission electron microscopy (JEM-2100 F, Japan) with an acceleration voltage of 200 kV and energy dispersive X-ray spectroscopy.

Laser Raman spectra were measured from 100 to 2000 cm^{-1} on a SPEX-1403 laser Raman spectrometer (SPEX Co., USA) using a 514.5 nm argon laser.

The zeta potentials of the series of Cu_2O-MoS_2 composites were recorded by a nanoparticle analyzer (Nano-ZS90, Malvern) at ambient temperature (Piao et al., 2014).

The morphologies of Cu_2O-MoS_2 hybrids in the polymer matrix were analyzed with transmission electronmicroscopy. The specimens were embedded in epoxy resin, and cut into thin films with a thickness of ca. 70 − 90 nm by ultramicrotomy at 25 °C.

The density of samples was tested according to ASTM D1622. The size of the specimen for the measurement was 30 × 30 × 30 mm^3, and the average density was received from at least five specimens. In addition, compressive properties of RPUF nanocomposites were characterized with a universal testing machine (Instron 1185) at room temperature. Values reported herein were the average of 5 tests.

Combustion properties of RPUF and its composites were performed on a microscale combustion calorimeter (MCC, GOVMARK) and thermal stability of the foams was performed by thermogravimetric

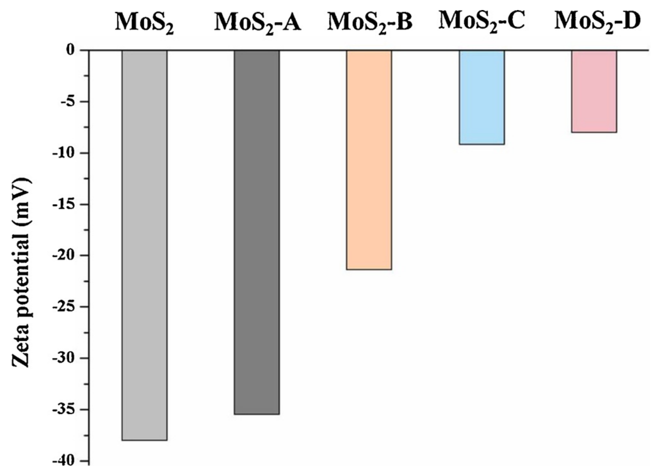

Fig. 3. The zeta potential of MoS_2, MoS_2-A, MoS_2-B, MoS_2-C and MoS_2-D hybrids when the weight ratio of MoS_2 and $Cu(CH_3COO)_2{\cdot}H_2O$ was 1:0, 1:1, 1:1.5, 1:2, 1:3.

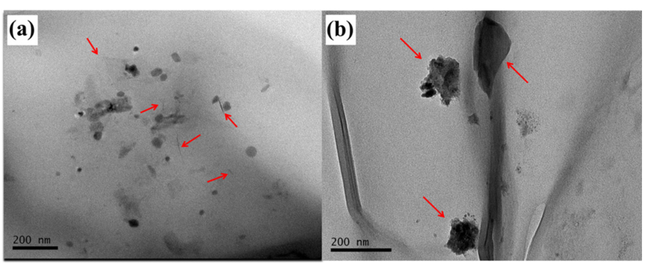

Fig. 4. TEM ultrathin observations of the RPUF/Cu_2O-MoS_2 composite (a) and RPUF/Cu_2O-MoS_2-M composite (b).

analysis (TGA) using a Q5000IR thermo-analyzer instrument at a linear heating rate of 20 °C min^{-1} from 30 °C to 800 °C under nitrogen or air condition.

Cone calorimeter (Stanton Redcroft, UK) tests were performed according to ISO 5660 standard. Each specimen was wrapped with aluminum foils and exposed to an external heat flux of 35 kW/m^2 with the size of 100 × 100 × 3 mm^3.

Scanning electron microscopy (Gemini500, ZEISS Co., German) was conducted to study the microstructures of the char residues of RPUF composites after cone calorimeter. The sample was coated with gold/palladium alloy.

Thermogravimetric analysis/infrared spectrometry (TG-IR) of RPUF and RPUF composites was carried out through a TGA Q5000 thermogravimetric analyzer, which used a stainless steel transfer pipe to combine with a Nicolet 6700 spectrophotometer. Thermal analyzer was conducted in the range from 25 to 500 °C with a heating rate of 20 °C/min under nitrogen condition.

Smoke toxicity was analyzed using a steady state tube furnace tests (SSTF) which was assessed on the basis of the ISO TS 19700. 20 g of samples in the form of granules were distributed evenly along the combustion quartz boat in the tube furnace with 825 °C at a constant rate. The air flow rate of 3.5 L min^{-1} went through the tube furnace to promote combustion.

The quantitative measurement of the evolved gases like CO, CO_2, NO_x and HCN was conducted by the tubular furnace method. 0.5 g of samples loaded into the crucible are fed into the furnace with 800 °C for at least 18 min. The combustion gases were continuously extracted using a pump with 2 L min^{-1}. A series of tests have been performed. Subsequently, specific analyzers containing nondispersive infrared detectors for CO_2, CO, NO_x and HCN were located at the end of the line.

3. Results and discussion

3.1. Structural characterization and morphology

Scheme 1 displays the typical synthesis and possible mechanism of Cu_2O-MoS_2 hybrids. At first, the bulk MoS_2 is inserted with metal ions (Li^+) by the solvothermal treatment, followed by exfoliation to form a single or few-layer nanosheet in deionized water through hydrolysis

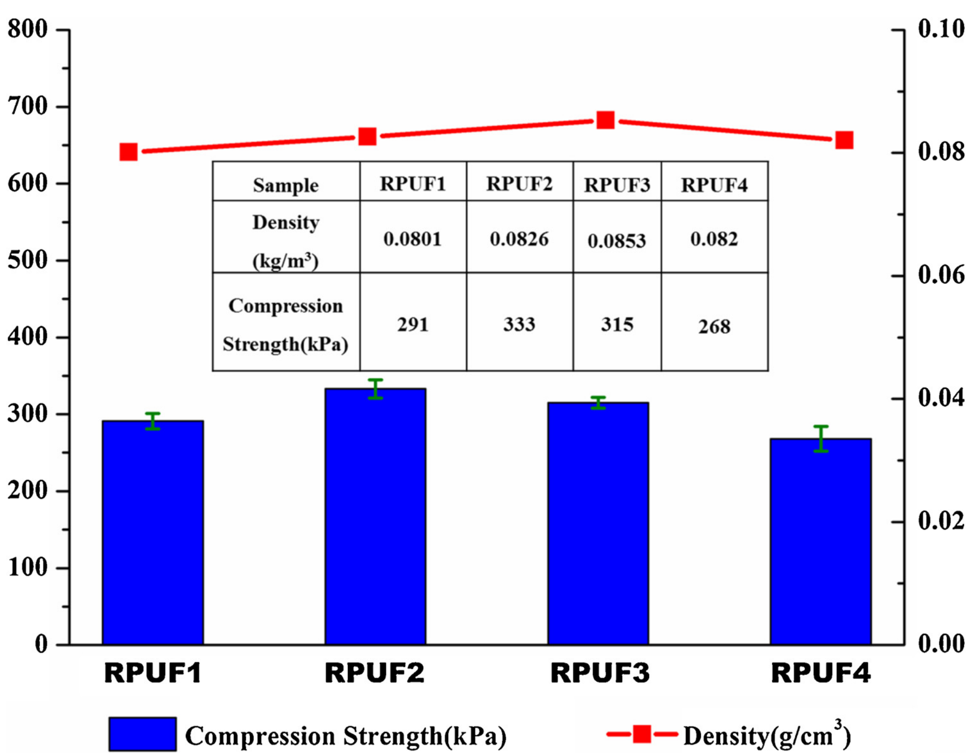

Fig. 5. Compressive strength and density of pristine RPUF, RPUF/MoS_2, RPUF/Cu_2O-MoS_2-L, RPUF/Cu_2O-MoS_2 and RPUF/Cu_2O-MoS_2-M composites.

Table 2
Compressive strengths of RPUF formulations and reported literatures.

Formulation	ΔCompressive strength (%)	Ref.
RPUF/HGM10-EG0-20 wt%	−70.68	*J. Appl. Polym. Sci. 109 (2008) 1935-1943* (Bian et al., 2008)
RPUF/pEG-PMMA-10 wt%	−10.39	*Polym. Degrad. Stab. 94 (2009) 971-979* (Ye et al., 2009)
RPUF/EG-10 wt%	−16%	*J. Appl. Polym. Sci. 114 (2009) 853-863* (Meng et al., 2009)
RPUF/APP-10 wt%	−32%	*J. Appl. Polym. Sci. 114 (2009) 853-863* (Meng et al., 2009)
PU/PFAPP/PL20 wt%	8.15%	*J. Polym. Res. 20 (2013) 234* (Xing et al., 2013)
RPUF/CNTs-0.3 wt%	16%	*Polym. Int. 61 (2012) 1107-1114* (Yan et al., 2012)
RPUF/Cu_2O-2 wt%	11.8%	*Composites Part A 112 (2018) 142–154* (Yuan et al., 2018b)
RPUF/MoO_3-2 wt%	11.7%	*Composites Part A 112 (2018) 142–154* (Yuan et al., 2018b)
RPUF/Cu_2O-MoS_2-1 wt%	8.3%	*This work*

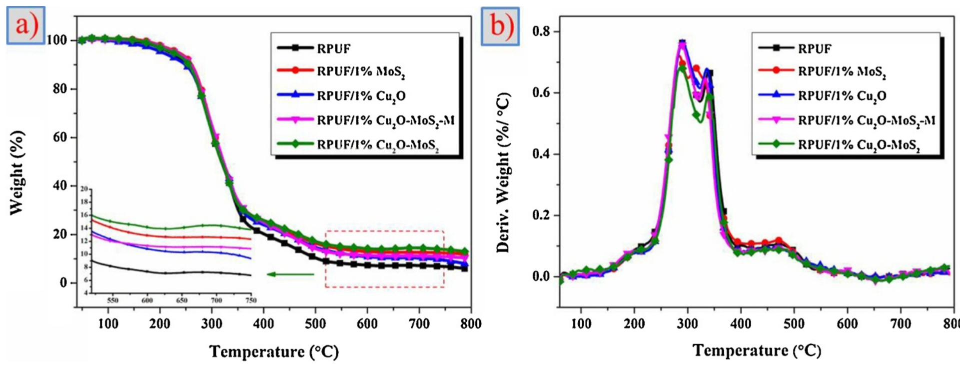

Fig. 6. TG/DTG profiles of pristine RPUF, RPUF/MoS_2, RPUF/Cu_2O, RPUF/Cu_2O-MoS_2-M and RPUF/Cu_2O-MoS_2 composites under nitrogen atmosphere.

Table 3
TGA results of pristine RPUF, RPUF/MoS_2, RPUF/Cu_2O-MoS_2 and RPUF/Cu_2O-MoS_2-M composites under nitrogen atmosphere.

Samples	$T_{-5\%}$ (°C)	$T_{-50\%}$ (°C)	Residue (wt%)
RPUF	218	318	5.85
RPUF/MoS_2	230	322	10.32
RPUF/Cu_2O-MoS_2-M	205	320	7.85
RPUF/Cu_2O-MoS_2	236	323	11.82

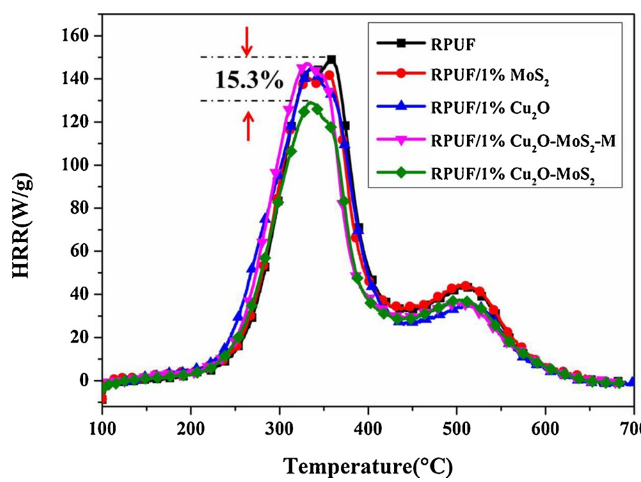

Fig. 7. The heat release rate (HRR) curves of pristine RPUF, RPUF/MoS_2, RPUF/Cu_2O, RPUF/Cu_2O-MoS_2 and RPUF/Cu_2O-MoS_2-M composites.

reaction. Then, a series of Cu_2O-MoS_2 hybrids with strong interfacial interaction are well obtained by a very facile wet chemical method. Specifically, the Cu^{2+} ions are attached to the surface of MoS_2 nanosheets by electrostatic attraction and the $Cu(OH)_2$ nanoparticulates will be transformed with the introduction of $N_2H_4{\cdot}H_2O$. Thus the self-assembly of Cu_2O-MoS_2 hybrids are acquired.

Fig. 1 displays the X-ray diffraction (XRD) patterns of the Cu_2O-MoS_2 hybrids and the re-stacked MoS_2. In the XRD pattern of Cu_2O, five narrow peaks appeared at 2θ of 29.5, 36.3, 42.3, 61.3 and 73.5° with lattice distance a = 4.269 Å (JCPDS file no. #05–0667) corresponding to the (110), (111), (200), (220) and (311) reflections, respectively. Compared with pristine MoS_2, the peaks indexed at 2θ = 36.3°, 42.3°, and 61.3° are observed for Cu_2O-MoS_2 hybrids, which were attributed to typical diffraction peaks of Cu_2O. For as-prepared Cu_2O-MoS_2 hybrids, the characteristic peaks at 14.1, 32.5, 40.0, and 59.0° are consistent with (002), (100), (103), and (110) crystal planes of the MoS_2 with high crystallinity, indicating the formation of Cu_2O crystalline phase on the surface of MoS_2. Moreover, the intensity of the diffraction peak for (002) (MoS_2) in the Cu_2O-MoS_2 hybrid decreases, indicating that the face-to-face stacking is broken due to the deposition of Cu_2O on both sides of MoS_2 nanosheets.

In order to further illustrate the phase of the Cu_2O-MoS_2 hybrid, Raman spectrum of Cu_2O-MoS_2 hybrid is also analyzed in detail, as shown in Fig. 1b. The characteristic peak at 381 cm^{-1} is associated with the in-plane E^1_{2g} vibration modes of two sulfur atoms with the molybdenum atom, while the peak at 407 cm^{-1} is attributed to the out-of-plane A_{1g} vibration modes of sulfur atoms (Lee et al., 2010; Fan et al., 2015; Coleman et al., 2011). Notably, the Raman shifts of Cu_2O at 218, 154 and 628 cm^{-1} appear in accordance with a second-order overtone and two infrared-allowed modes respectively after the loading of Cu_2O on MoS_2 nanosheets (Powell et al., 1975; Li et al., 2017). Meanwhile, the vibrational fingerprint at 218 cm^{-1} of Cu_2O-MoS_2 sample should be assigned to T_{2u} and Raman scattering features from Cu_2O (Fan et al., 2016; Hardcastle, 2011; Prabhakaran and Murugan, 2014; Ohsaka et al., 1978).

TEM was applied to reveal the morphology and structure information of MoS_2 and Cu_2O-MoS_2. As depicted in Fig. 2a, two-dimensional MoS_2 presents a typical platelet shape with several hundred nanometers large, which certifies that the MoS_2 is fully exfoliated into thin layers. As for the Cu_2O-MoS_2-L (less loading of Cu_2O) hybrid, only a tiny fraction of Cu_2O nanoparticles are anchored on the surface of MoS_2 nanosheets (Fig. 2b). It is noteworthy that the Cu_2O-MoS_2-L hybrid displays an exfoliated layer with a fairly low loading of Cu_2O. From

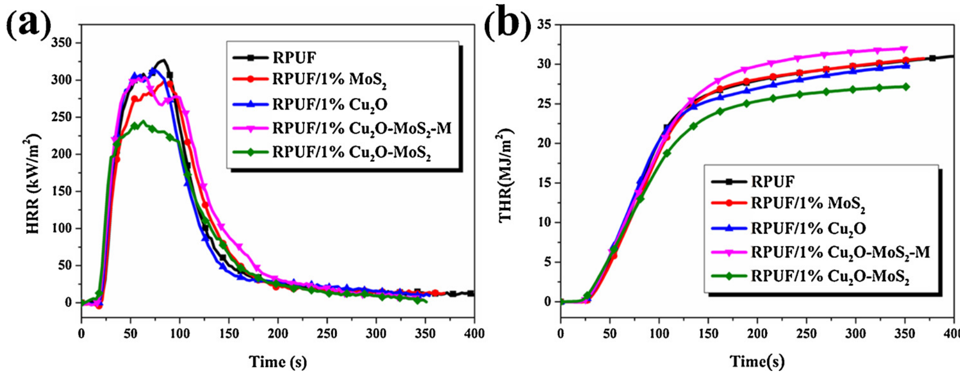

Fig. 8. Heat release rate (a) and total heat release (b) versus time curves of pristine RPUF and its composites.

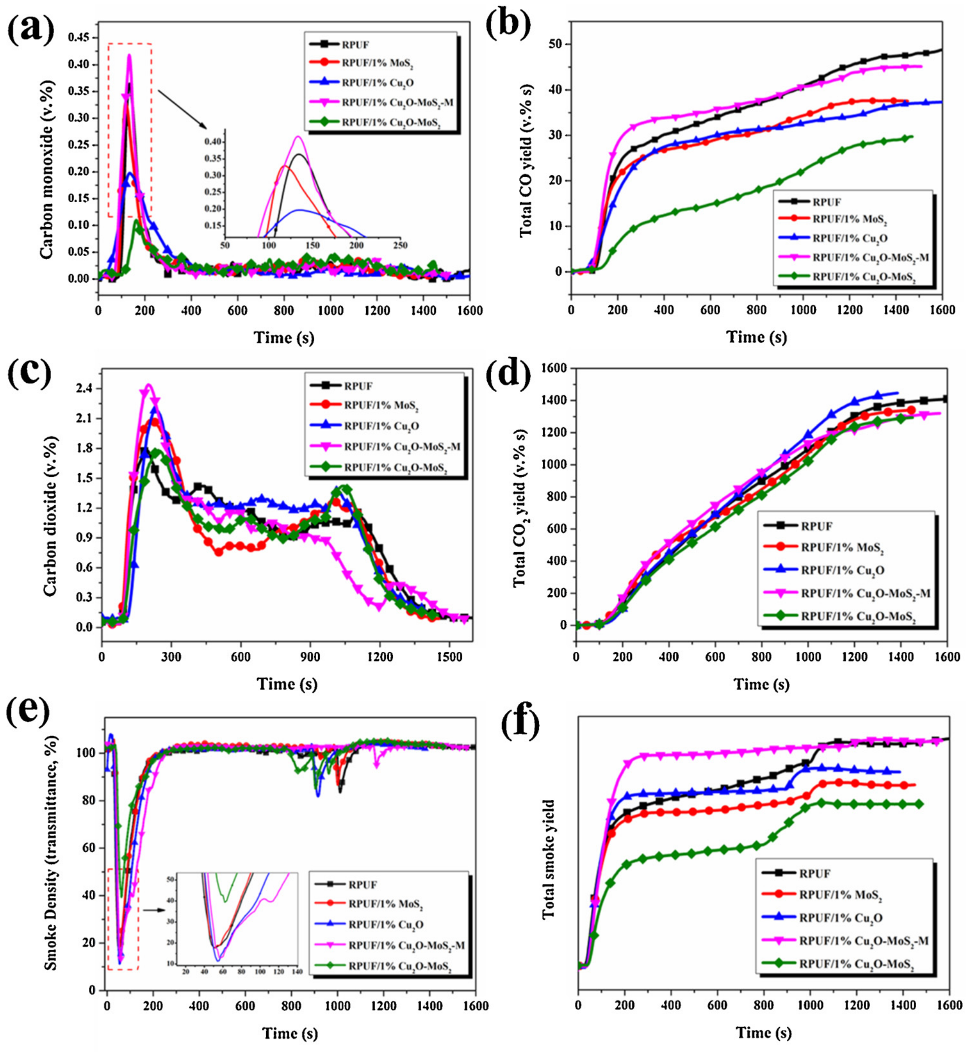

Fig. 9. CO curves (a, b), CO_2 curves (c, d), and total smoke density (e, f) of pristine RPUF and its composites obtained from SSTF tests.

Fig. 2c, the Cu_2O nanoparticles are uniformly and firmly decorated on the surface of the MoS_2 nanosheets. Compact lamellar structures and no aggregations of the MoS_2 nanolayers can be seen for the Cu_2O-MoS_2 hybrids, demonstrating that the Cu_2O nanoparticles are anchored stiffly on the surface of MoS_2 nanosheets. As seen In Fig. 2d, the morphology of the Cu_2O-MoS_2-M hybrid displays abundant layers tangle. The restacking of MoS_2 nanosheets is probably attributed to the presence of vast numbers of positive charges by Cu^{2+} ions precipitating on the surface of MoS_2 nanosheets during preparation. For further confirmation of the Cu_2O-MoS_2 hybrids, Fig. 2e displays the elementary composition of the selected fields by energy dispersive X-ray spectroscopy (EDX). It is noticeable that the Mo, S, Cu and O elements existed in Cu_2O-MoS_2 hybrid. Notably, the C and Al peaks are derived from the aluminum grids (Cherstiouk et al., 2016). Hence, the emergence of O and Cu is due to the Cu_2O nanoparticles attached to the surface of the MoS_2 nanosheets. The atomic ratios of Mo, S and Cu are inserted in Fig. 2e and the EDX spectrum farther indicates that the Cu_2O-MoS_2 hybrid was successfully prepared.

Table 4
Quantitative analysis of gaseous products of degradation of pristine RPUF, RPUF/MoS_2, RPUF/Cu_2O-MoS_2 and RPUF/Cu_2O-MoS_2-M composites by tubular furnace method at 825 °C.

Samples	Products					N-Gas value Eqn.(1)
	HCN (ppm)	NO_x (ppm)	CO (ppm)	CO_2 (ppm)	O_2 (ppm)	
RPUF	325	30	5000	115000	18.3	1.079
RPUF/MoS_2	335	24	4900	100000	18.6	1.095
RPUF/Cu_2O-MoS_2-M	320	34	5200	105000	18.7	1.154
RPUF/Cu_2O-MoS_2	275	14	3600	120000	17.9	0.787

To ascertain the TEM results, the zeta potential of a series of Cu_2O-MoS_2 hybrids with the same concentration was measured. Generally, the zeta potential is an important parameter for characterizing the stability of colloidal dispersions and provides a measure of the magnitude and sign of the effective surface charge associated with the double layer around the colloid particle (Gupta et al., 2015). Generally, particles with zeta potentials more positive than +30 mV or more negative than −30 mV are considered to form stable dispersions due to interparticle electrostatic repulsion. Fig. 3a exhibits the pristine MoS_2 nanosheets achieve a fairly high negative charge (-37.5 ± 2.5 mV) on the surface. Nevertheless, the surface charge begins to go up and reaches -21.3 mV with the loading of appropriate Cu^{2+} ions. More importantly, the addition of Cu^{2+} ions with a high loading can severely decreases the negative potential from 21.3 to 8.9 mV. In addition, significant face-to-face stacking is broken due to the reduced van der Waals forces by the introduction of Cu_2O nanoparticles. Consequently, the self-assembly of the Cu_2O-MoS_2 hybrid is unfavorable due to the less electrostatic repulsion of interlamination of MoS_2 nanosheets (Gupta et al., 2015).

3.2. Mechanical properties of RPUF composites

3.2.1. Dispersion state of Cu_2O-MoS_2 hybrids in RPUF composites

The interfacial interaction and dispersion of nanofillers in polymers reveal a key factor to influence the performance of polymeric nanocomposites (Bao et al., 2011; Yuan et al., 2018a). To assess the dispersion states of different Cu_2O-MoS_2 hybrids in the RPUF nanocomposites, the morphologies of fractured surfaces were analyzed using TEM, as portrayed in Fig. 4. The Cu_2O-MoS_2 hybrids are finely dispersed and embedded in the RPUF without aggregation under higher magnification (Fig. 4a). By comparison, after the incorporation of Cu_2O-MoS_2-M hybrids, the hybrids agglomerate severely in the RPUF nanocomposites, which are probably attributed to a forceful van der Waals and intralayer covalent bonding with the presence of vast numbers of positive charges promoting the restacking of MoS_2 nanolayers in the RPUF nanocomposites during preparation.

3.2.2. Foam density and compressive strength

Basically, the compressive strength of the RPUF composites will be enhanced if the nanoadditives are finely distributed in the RPUF substrate because of the superior interaction between the nanoadditives and polymers. As portrayed in Fig. 5, a distinct improvement in compressive strength is obtained with the introduction of the Cu_2O-MoS_2 hybrid. Compared with the data from Table 2, the compressive strength increases effectively, which is possibly due to the highly dispersed Cu_2O-anchored MoS_2 have an enormous number of hydroxyl groups to form the crosslinking system with favorable compatibility between the nanoparticles and RPUF matrix (Huang et al., 2013; Yuan et al., 2018b), which promote its excellent dispersion in the matrix, improving the mechanical property between the Cu_2O-MoS_2 hybrid and RPUF matrix. The sample with 1% concentration of Cu_2O-MoS_2-M hybrid shows a decrease of 7.9% in the compressive strength, which should be attributed to the poor compatibility between the Cu_2O-MoS_2-M hybrid and RPUF matrix (Wang et al., 2016). Incorporating Cu_2O-MoS_2 hybrid into the RPUF matrix leads to an increase of 8.3% in the compressive strength, achieving the purpose of reinforcement for the RPUF matrix (Thirumal et al., 2007). Compared with the data from Table 2, the compressive strength increases effectively, which is possibly due to the highly dispersed Cu_2O-anchored MoS_2 hybrids have hydroxyl group can react with the R-NCO groups of isocyanurate to form the crosslinking system with favorable compatibility between the particles and the matrix

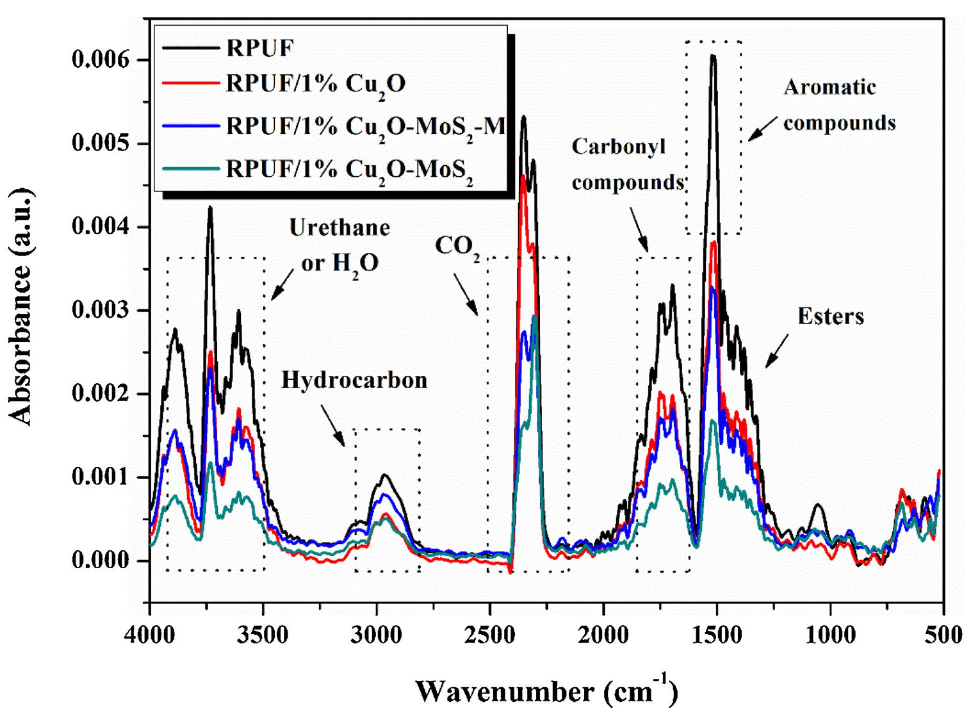

Fig. 10. TG-IR spectra of pyrolysis products of pristine RPUF, RPUF/Cu_2O, RPUF/Cu_2O-MoS_2 and RPUF/Cu_2O-MoS_2-M composites at maximum decomposition rate.

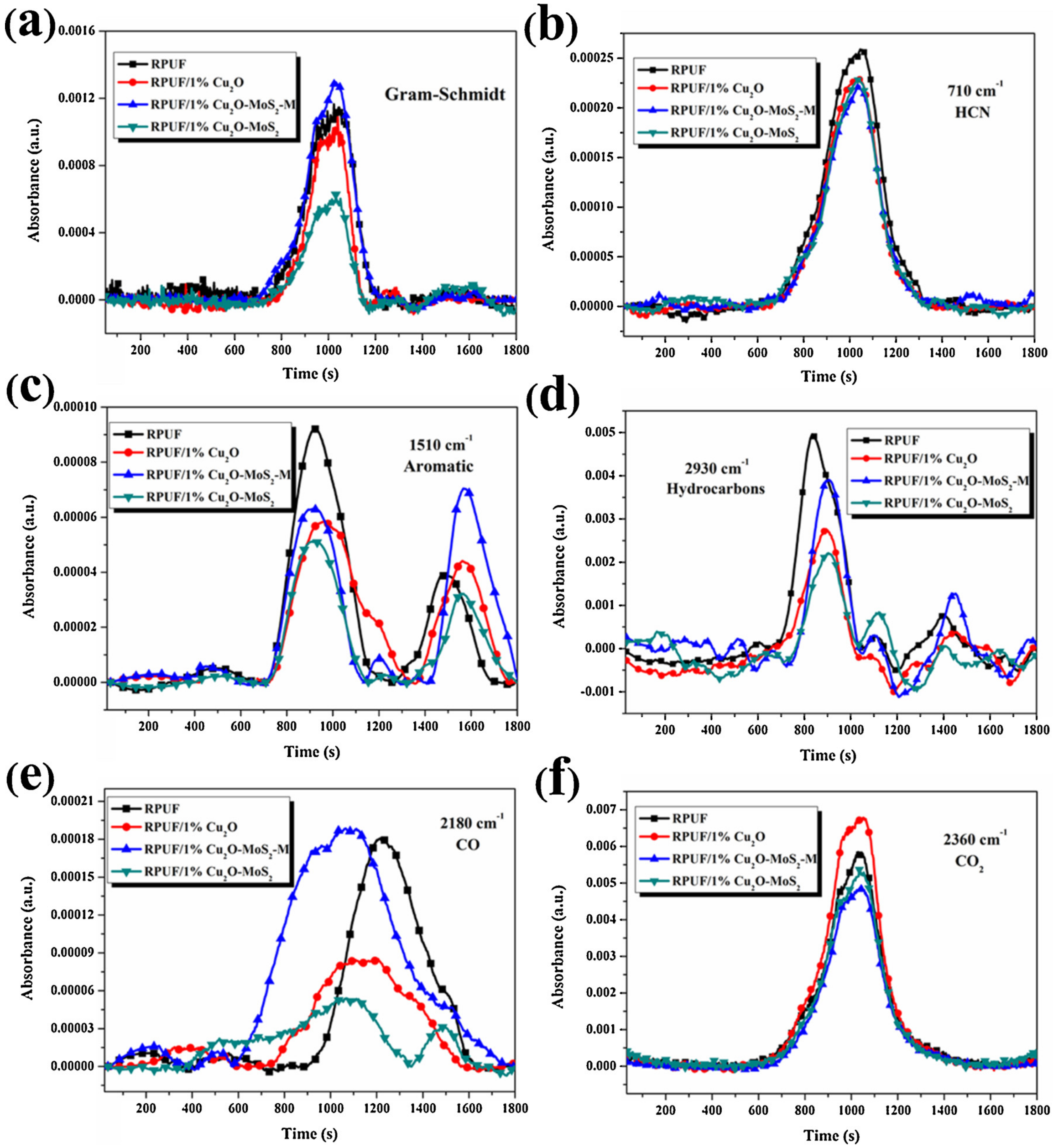

Fig. 11. Gram–Schmidt curves (a) and Intensity of characteristic peaks for pyrolysis products of pristine RPUF, RPUF/Cu_2O, RPUF/Cu_2O-MoS_2 and RPUF/Cu_2O-MoS_2-M composites at maximum decomposition rate (b)-(f).

3.3. Thermal property

The influence of Cu_2O-MoS_2 hybrid on the thermal stability property of RPUF was analyzed by TGA. The TGA curves of RPUF/MoS_2, RPUF/Cu_2O, RPUF/Cu_2O-MoS_2 and RPUF/Cu_2O-MoS_2-M composites in anaerobe conditions are described in Fig. 6. In addition, the typical thermal parameters were presented in Table 3. It is noticeable that the pyrolysis process under anaerobe atmosphere includes two-stage steps referred to the DTG profile (Camino et al., 1984). As can be observed from Fig. 6a, the first step occurs in the ranges of 223–422 °C, which derives from the degradation of hard-segment (Chattopadhyay and Webster, 2009). The weak C—NH bond brings about the generation of isocyanate primary or secondary amine and alcohol (Yuan et al., 2016). The subsequent step is ascribed to the decomposition of the soft-segment which contains a stable urea structure (Modesti et al., 2008). Interestingly, a 18 °C increment and a 13 °C decrement in $T_{-5\%}$ are observed for RPUF/Cu_2O-MoS_2 and RPUF/Cu_2O-MoS_2-M respectively, rivaled by pristine RPUF. It could be caused by the restacking of MoS_2 for the Cu_2O-MoS_2-M hybrid (Bissessur et al., 1993). The TG results present that the residues of RPUF/MoS_2, RPUF/Cu_2O-MoS_2 and RPUF/Cu_2O-MoS_2-M composites are much more than that of pristine RPUF (5.85 wt%), which are 10.32 wt%, 7.85 wt% and 11.82 wt%, respectively, revealing that the Cu_2O-MoS_2 possess impressive catalytic charring behavior for RPUF. Additionally, as seen from DTG curves, the maximum mass loss rate of the RPUF/Cu_2O-MoS_2 is the lowest, indicating that the barrier effect and catalytic charring of Cu_2O-MoS_2 hybrid plays an important role in enhancing thermal stability significantly (Cao et al., 2010).

3.4. Fire hazards

3.4.1. Flammability of RPUF composites

MCC is a valid laboratory test to evaluate RPUF and its composites for their fire-retardant property. The heat release rate curves of pristine

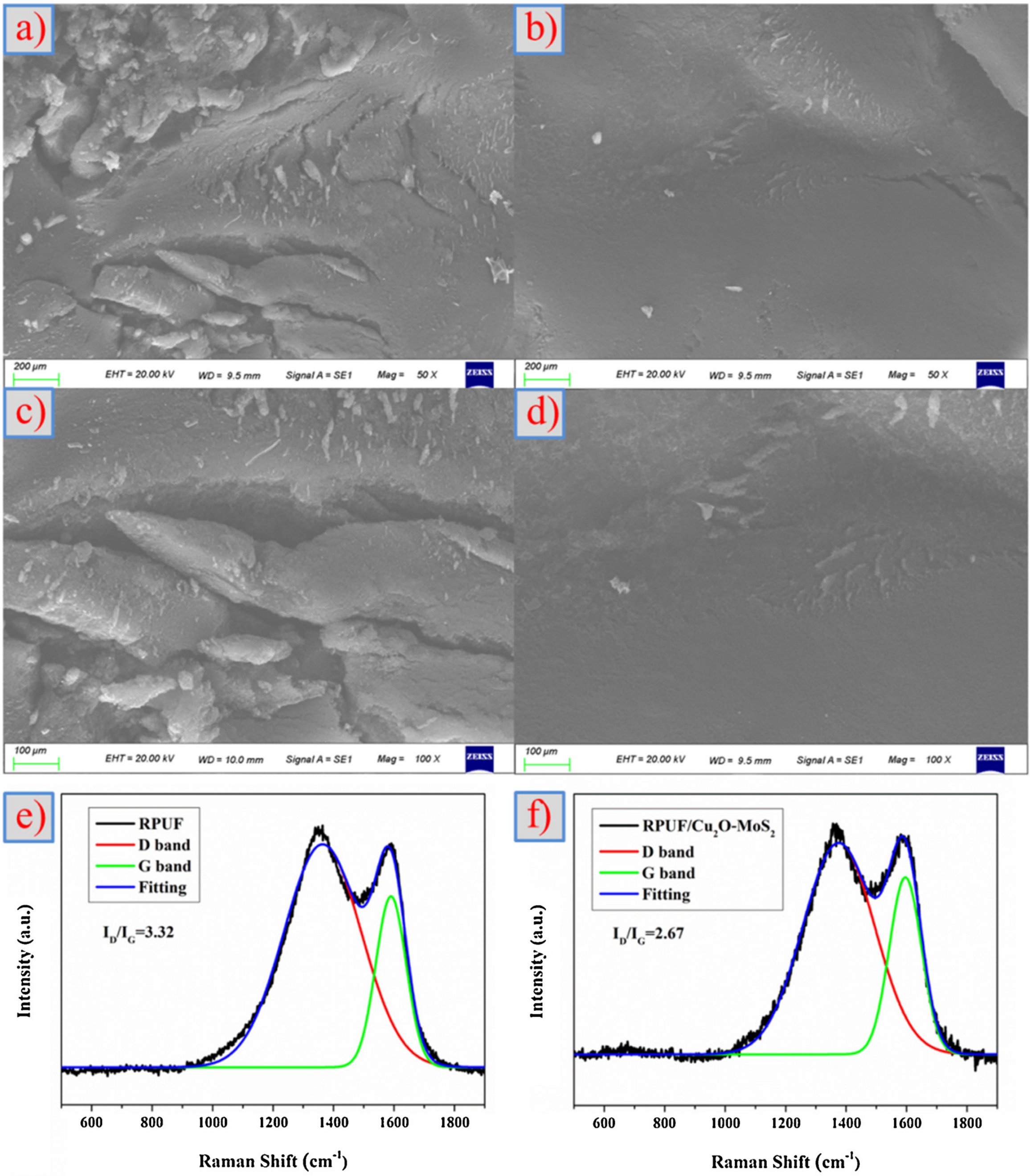

Fig. 12. SEM micrographs (a–d) and Raman spectra (e–f) of the surface residues from pristine RPUF (a, c) and RPUF/Cu2O-MoS2 (b, d) after cone calorimeter tests.

RPUF, RPUF/MoS_2, RPUF/Cu_2O, RPUF/Cu_2O-MoS_2 and RPUF/Cu_2O-MoS_2-M composites are portrayed in Fig. 7. A decrease of 15.3% in the peak heat release rate (pHRR) for RPUF/Cu_2O-MoS_2 composite is obtained, compared to pristine RPUF, which is ascribed to the layered barrier effect and catalytic carbonization of the Cu_2O-MoS_2 hybrids. Unfortunately, only slight decrease in pHRR is observed when the Cu_2O-MoS_2-M hybrids are incorporated into RPUF. These results certify that the thin layer structure of MoS_2 nanosheets have significant effect on decreasing the pHRR.

To evaluated the influence of incorporation of Cu_2O-anchored MoS_2 hybrids on the combustion behaviors of RPUF composites, HRR and THR curves of pristine RPUF and its composites are plotted in Fig. 8. It is noticeable that the addition of pristine MoS_2 and Cu_2O (1 wt%) gives rise to a 9.8% and 3.6% reduction in pHRR, Furthermore, incorporating 1 wt% Cu_2O-MoS_2 into RPUF results in the lowest peak HRR value (26.3% reduction). Also, the addition of 1 wt% Cu_2O-MoS_2 gives rise to the lowest total heat release (THR) and highest char yield. The mechanism of Cu_2O-MoS_2 in reducing the flammability of RPUF is probably attributed to the barrier effect and charring effect which could obtain a protective char and slow down the heat and mass transfer.

3.4.2. Smoke toxicity analysis by SSTF

To better realize the roles of the MoS_2, Cu_2O, Cu_2O-MoS_2 and Cu_2O-MoS_2-M on decreasing the smoke toxicity, the steady state tube furnace test were performed on pristine RPUF and its nanocomposites. It is well known that rigid polyurethane foam is easily combustible and produces a great deal of smoke and toxic gases. Accordingly, the reduction of the amount of toxic gases and smoke has significant influence on saving lives during combustion process. Fig. 9 exhibits the curves of CO, CO_2 and smoke yield as a function of time for the RPUF nanocomposites

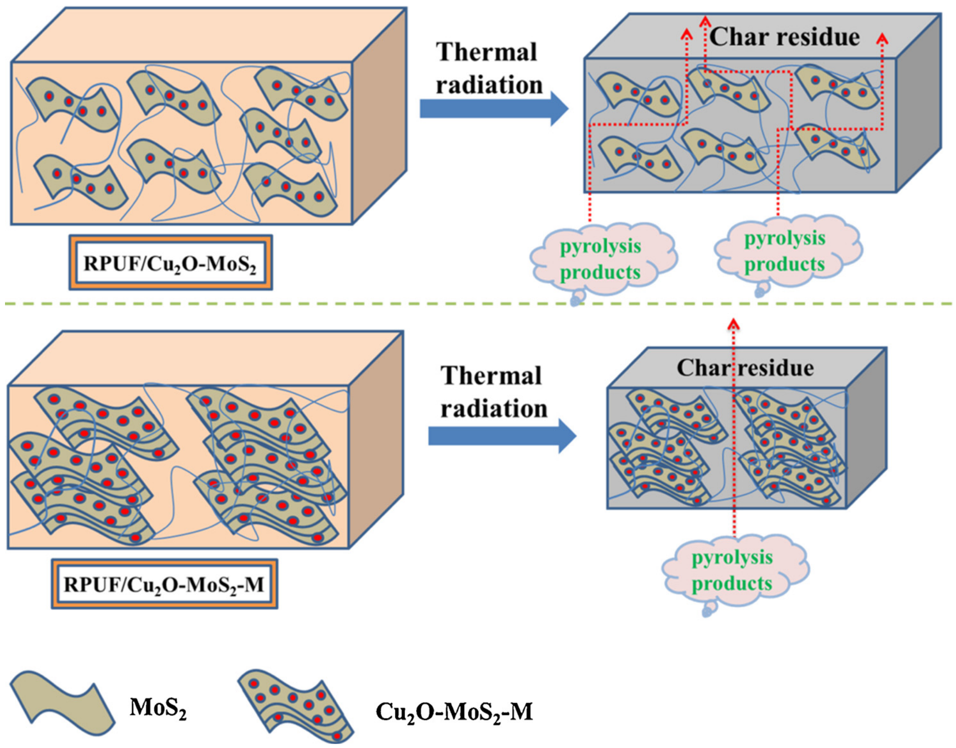

Fig. 13. Schematic illustration for the mechanism of catalytic oxidation of the Cu_2O-MoS_2 hybrids in the thermal degradation process of the RPUF composite.

derived from SSTF results. As seen in Fig. 9, RPUF/MoS_2 depicts mildly decreased CO yields and smoke density compared with pristine RPUF. It is attributed to the physical adsorption effect of the thin layer structure of MoS_2 nanosheets with huge specific surface area (Wang et al., 2014b). CO concentration for RPUF/Cu_2O is reduced, while the CO_2 yields have been increased for the nanocomposites as compared to that of pristine RPUF, indicating that the catalytic oxidation of Cu_2O is certified under air atmosphere. Specifically, the CO yields and smoke during combustion for the sample with Cu_2O-MoS_2 hybrid are dramatically decreased compared to pristine RPUF. The reduction should be derived from the synergistic effect between the adsorption of MoS_2 and the restricted mobility in the polymer chains by the restriction of Cu_2O (Laachachi et al., 2007, 2005). MoS_2 is apt to absorb small gaseous molecules, thus retarding the escape of the organic volatiles to form smoke, owing to the physical adsorption effect. Meanwhile, the Cu_2O nanoparticles catalyze the oxidation of organic volatiles, thereby decreasing the fire hazards.

3.4.3. Volatile gases analysis by tubular furnace test

To investigate the adsorption and catalytic oxidation behavior of Cu_2O-MoS_2 hybrid to reduce the fire hazards of RPUF nanocomposites, the amounts of toxic gases were gathered to measure the composition from the tubular furnace experiments. It can be seen from Table 4, with the addition of Cu_2O-MoS_2 hybrids into RPUF, the acquisition of toxic gases during thermal degradation in open porcelain pans set in a tube furnace is decreased substantially. The introduction of Cu_2O-MoS_2 hybrids retards the evolution of principal toxicants (CO and NO_x) significantly compared to other samples which is considered as an important finding. The lower yield of principal toxicants and the higher yield of CO_2 indicate that Cu_2O-MoS_2 is an efficient catalyst which can accelerate the reaction of CO and NO_x to produce desired harmless gases during decomposition of RPUF (Shi et al., 2015).

The toxicants were predicted by NIST according to the N-Gas model in Eqn. (1). This model expresses the ratio of the concentration of each toxicant to its lethal concentration, and then multiplies the sum of this ratio by the hyperventilation factor (Stec and Hull, 2011). Generally, animal deaths will start to occur when the N-Gas value is above 0.8 and 100% of the animals will die when the value is above 1.3 (Liu et al., 2016). The results of this experiment according to Eqn. (1) are presented in Table 4, which indicate that the incorporation of Cu_2O-MoS_2 hybrids for reducing the fire hazards is significantly enhanced.

3.4.4. Evolved gases analysis by TG-IR

TG—IR was employed to analyze the evolved volatiles of RPUF and RPUF nanocomposites during thermal decomposition process and explore the mechanism of smoke toxicity suppression. The FTIR spectra of pyrolysis products at maximum degradation rate during the pyrolysis of RPUF, RPUF/Cu_2O, RPUF/Cu_2O-MoS_2 and RPUF/Cu_2O-MoS_2-M nanocomposites are presented in Fig. 10. Peaks in the range of 3850-3550 cm^{-1} are assigned to the vibrations of O—H stretch bond of water or N—H stretch bond in urethane. It is obvious that the emergence of vibrations at 1238, 1505, 2185, 2358 and 2920 cm^{-1} derive from esters, aromatic compounds, CO, CO_2 and hydrocarbons.

To further understand the changes of the pyrolysis products, the relative intensity of the pyrolysis gases of pristine RPUF and its nanocomposites are depicted in Fig. 11. From Gram–Schmidt curve, it is clearly observed that the Cu_2O-MoS_2 hybrids into RPUF can change the thermal degradation process and bring about a depressed emission of pyrolysis products (Cao et al., 2010). Meanwhile, the dramatical reduction of fire hazards and toxic gases for RPUF/Cu_2O-MoS_2 nanocomposite lead to a decrement in the fire hazard, which will reduce the smoke toxicity of RPUF and be beneficial for fire rescue.

3.5. Char residue analysis

Fig. 12 presents the SEM images of the char residues for pristine RPUF and RPUF/Cu_2O-MoS_2 after cone calorimeter tests. It can be depicted from Fig. 12(a–d), the char residue of pristine RPUF exhibits relatively loose and fragile with many cracks from Fig. 12(a–d), which cannot act as a shielding effect to protect the polymer matrix. In contrast, RPUF/Cu_2O-MoS_2 nanocomposites obtain compact char residues during combustion, which can hinder the flammable gases and afford better shielding action. To investigate the condensed-phased products of RPUF nanocomposites after combustion, Fig. 12 shows the Raman spectra of the surface residues of RPUF and RPUF/Cu_2O-MoS_2 nanocomposites. The spectra display similar shape overlapping peaks at approximately 1595 and 1360 cm^{-1}, which belongs to G band and D band (Fang et al., 2010). The intensity ratio of the G to D band (I_G/I_D) of RPUF/Cu_2O-MoS_2 is higher than that of pristine RPUF, suggesting that the introduction of Cu_2O-MoS_2 hybrids could form compact graphitic char residues, which act as a useful barrier and protect underlying material.

On the basis of the above-mentioned results, the mechanism for the improvement of thermal stability and the reduction of smoke toxicity of RPUF/Cu_2O-MoS_2 nanocomposite is illustrated in Fig. 13 and proposed as follows: (i) the physical adsorption effect of MoS_2 and the restricted mobility of the polymer chains by the restriction effect of Cu_2O is responsible for enhancing the thermal stability; (ii) the synergistic effect between the physical adsorption of MoS_2 and the catalysis action of Cu_2O play a synergistic role in decreasing the fire hazards. Additionally, the synergistic effect of RPUF/Cu_2O-MoS_2-M nanocomposite is inferior to those of RPUF/Cu_2O-MoS_2 nanocomposite, which provides direct proofs of the negative influence of the stacked MoS_2 on reducing the smoke toxicity for RPUF nanocomposites.

4. Conclusions

In the present study, layered MoS_2 decorated with Cu_2O nanoparticles has been prepared to decrease smoke toxicity for RPUF nanocomposites. The results indicate that the activity of the layered MoS_2 for reducing the fire hazards is markedly improved with the addition of the Cu_2O cocatalyst. The structural and morphology characterization illustrate that the surface of layer-structured material was decorated with Cu_2O nanoparticle successfully. Moreover, the results suggest that the Cu_2O-MoS_2 hybrid effectively prevented the MoS_2 nanosheets from restacking but Cu_2O-MoS_2-M hybrid displayed a characteristic stacked layer structure. TGA investigation exhibited that the thermal stability of RPUF is markedly improved by adding Cu_2O-MoS_2 hybrid at a low loading (1 wt%) and the physical adsorption and catalytic carbonization of Cu_2O-MoS_2 hybrids are believed to be important factors. Furthermore, catalytic oxidation of Cu_2O-MoS_2 hybrids on thermal decomposition and generation of toxic gases of RPUF was studied by TG-IR and SSTF and calculated by N-Gas model. It was found that the amounts of the toxic organic volatiles were decreased owing to the synergistic effect between the physical adsorption of MoS_2 and the catalysis action of Cu_2O. The work depicts that the development of noble-metal-free layer-structured composites, such as Cu_2O-MoS_2 hybrid, containing an inexpensive and environmentally benign Cu_2O cocatalyst, is feasible and has great potential for reducing smoke toxicity of fire safety RPUF composites.

Acknowledgments

The work was financially supported by the National Key Research and Development Program of China (2017YFC0805901, 2016YFB0302104), National Natural Science Foundation of China (51761135113, 51803204) and China Postdoctoral Science Foundation (2018M642540).

References

Santos, O., da Silva, M.C., Silva, V., Mussel, W., Yoshida, M., 2017. Polyurethane foam impregnated with lignin as a filler for the removal of crude oil from contaminated water. J. Hazard. Mater. 324, 406–413.
Kacperski, M., Spychaj, T., 1999. Rigid polyurethane foams with poly (ethylene terephthalate)/triethanolamine recycling products. Polym. Adv. Technol. 10, 620–624.
Pauzi, N.N.P.N., Majid, R.A., Dzulkifli, M.H., Yahya, M.Y., 2014. Development of rigid bio-based polyurethane foam reinforced with nanoclay. Compos. Part B Eng. 67, 521–526.
Chattopadhyay, D., Webster, D.C., 2009. Thermal stability and flame retardancy of polyurethanes. Prog. Polym. Sci. 34, 1068–1133.
Zhang, M., Zhang, J., Chen, S., Zhou, Y., 2014. Synthesis and fire properties of rigid polyurethane foams made from a polyol derived from melamine and cardanol. Polym. Degrad. Stab. 110, 27–34.
Zhang, J., Kong, Q., Yang, L., Wang, D.-Y., 2016. Few layered $Co(OH)_2$ ultrathin nanosheet-based polyurethane nanocomposites with reduced fire hazard: from eco-friendly flame retardance to sustainable recycling. Green Chem. 18, 3066–3074.
Wang, D., Zhang, Q., Zhou, K., Yang, W., Hu, Y., Gong, X., 2014a. The influence of manganese–cobalt oxide/graphene on reducing fire hazards of poly (butylene terephthalate). J. Hazard. Mater. 278, 391–400.
Levchik, S.V., Weil, E.D., 2005. Flame retardancy of thermoplastic polyesters—a review of the recent literature. Polym. Int. 54, 11–35.
Carty, P., White, S., 1994. Flame retardancy and smoke suppression in a tertiary polymer blend. Polym. Degrad. Stab. 44, 93–97.
Ling, Z., Wan, P., Yu, C., Xiao, N., Yang, J., Long, Y., Qiu, J., 2015. One-pot to fabrication of calcium oxide/carbon foam composites for the adsorption of trace SO_2. Chem. Eng. J. 259, 894–899.
Yu, B., Xing, W., Guo, W., Qiu, S., Wang, X., Lo, S., Hu, Y., 2016. Thermal exfoliation of hexagonal boron nitride for effective enhancements on thermal stability, flame retardancy and smoke suppression of epoxy resin nanocomposites via sol–gel process. J. Mater. Chem.A 4, 7330–7340.
Sun, B.-Z., Chen, W.-K., Xu, Y.-J., 2010. Reaction mechanism of CO oxidation on Cu_2O (111): a density functional study. J. Chem. Phys. 133, 154502.
White, B., Yin, M., Hall, A., Le, D., Stolbov, S., Rahman, T., Turro, N., O'Brien, S., 2006. Complete CO oxidation over Cu_2O nanoparticles supported on silica gel. Nano Lett. 6, 2095–2098.
Kröcher, O., Elsener, M., 2009. Hydrolysis and oxidation of gaseous HCN over heterogeneous catalysts. Appl. Catal., B-Environ. 92, 75–89.
Moreno, J.L.V., Padama, A.A.B., Kasai, H., 2014. A density functional theory-based study on the dissociation of NO on a CuO (110) surface. CrystEngComm 16, 2260–2265.
Shi, Y., Yu, B., Duan, L., Gui, Z., Wang, B., Hu, Y., Yuen, R.K., 2017. Graphitic carbon nitride/phosphorus-rich aluminum phosphinates hybrids as smoke suppressants and flame retardants for polystyrene. J. Hazard. Mater. 332, 87–96.
Zhao, H., Tonkyn, R.G., Barlow, S.E., Koel, B.E., Peden, C.H., 2006. Catalytic oxidation of HCN over a 0.5% Pt/Al_2O_3 catalyst. Appl. Catal., B-Environ. 65, 282–290.
Sun, B.-Z., Xu, X.-L., Chen, W.-K., Dong, L.-H., 2014. Theoretical insights into the reaction mechanisms of NO oxidation catalyzed by Cu_2O (1 1 1). Appl. Surf. Sci. 316, 416–423.
Tu, H., Wang, J., 1996. An XPS investigation of thermal degradation and charring processes for PVC and PVC/Cu_2O systems in the condensed phase—II. Polym. Degrad. Stab. 54, 195–203.
Dinter, N., Rusanen, M., Raybaud, P., Kasztelan, S., da Silva, P., Toulhoat, H., 2009. Temperature-programed reduction of unpromoted MoS_2-based hydrodesulfurization catalysts: experiments and kinetic modeling from first principles. J. Catal. 267, 67–77.
Breysse, M., Geantet, C., Afanasiev, P., Blanchard, J., Vrinat, M., 2008. Recent studies on the preparation, activation and design of active phases and supports of hydrotreating catalysts. Catal. Today 130, 3–13.
Yu, B., Shi, Y., Yuan, B., Qiu, S., Xing, W., Hu, W., Song, L., Lo, S., Hu, Y., 2015. Enhanced thermal and flame retardant properties of flame-retardant-wrapped graphene/epoxy resin nanocomposites. J. Mater. Chem. A 3, 8034–8044.
Wang, X., Xing, W., Feng, X., Song, L., Hu, Y., 2017. MoS_2/Polymer nanocomposites: preparation, properties, and applications. Polym. Rev. Phila. Pa (Phila Pa) 57, 440–466.
Lee, C., Yan, H., Brus, L.E., Heinz, T.F., Hone, J., Ryu, S., 2010. Anomalous lattice vibrations of single-and few-layer MoS_2. ACS Nano 4, 2695–2700.
Yuwen, L., Xu, F., Xue, B., Luo, Z., Zhang, Q., Bao, B., Su, S., Weng, L., Huang, W., Wang, L., 2014. General synthesis of noble metal (Au, Ag, Pd, Pt) nanocrystal modified MoS_2 nanosheets and the enhanced catalytic activity of Pd–MoS_2 for methanol oxidation. Nanoscale 6, 5762–5769.
Feng, X., Xing, W., Song, L., Hu, Y., 2014. In situ synthesis of a MoS2/CoOOH hybrid by a facile wet chemical method and the catalytic oxidation of CO in epoxy resin during decomposition. J. Mater. Chem. A 2, 13299–13308.
Levin, B.C., 1996. New research avenues in toxicology: 7-gas N-gas model, toxicant suppressants, and genetic toxicology. Toxicology 115, 89–106.
Yang, M.-Q., Han, C., Xu, Y.-J., 2015. Insight into the effect of highly dispersed MoS_2 versus layer-structured MoS_2 on the photocorrosion and photoactivity of CdS in graphene–CdS–MoS_2 composites. J. Phys. Chem. C 119, 27234–27246.
Yuan, Y., Yang, H., Yu, B., Shi, Y., Wang, W., Song, L., Hu, Y., Zhang, Y., 2016. Phosphorus and nitrogen-containing polyols: synergistic effect on the thermal property and flame retardancy of rigid polyurethane foam composites. Ind. Eng. Chem. Res. 55, 10813–10822.
Piao, J.-G., Wang, L., Gao, F., You, Y.-Z., Xiong, Y., Yang, L., 2014. Erythrocyte membrane is an alternative coating to polyethylene glycol for prolonging the circulation lifetime of gold nanocages for photothermal therapy. ACS Nano 8, 10414–10425.
Fan, X., Xu, P., Zhou, D., Sun, Y., Li, Y.C., Nguyen, M.A.T., Terrones, M., Mallouk, T.E., 2015. Fast and efficient preparation of exfoliated 2H MoS_2 nanosheets by sonication-assisted lithium intercalation and infrared laser-induced 1T to 2H phase reversion. Nano Lett. 15, 5956–5960.
Coleman, J.N., Lotya, M., O'Neill, A., Bergin, S.D., King, P.J., Khan, U., Young, K., Gaucher, A., De, S., Smith, R.J., 2011. Two-dimensional nanosheets produced by liquid exfoliation of layered materials. Science 331, 568–571.
Powell, D., Compaan, A., Macdonald, J., Forman, R., 1975. Raman-scattering study of ion-implantation-produced damage in Cu_2O. Phys. Rev. 12, 20.
Li, Z., Pi, Y., Xu, D., Li, Y., Peng, W., Zhang, G., Zhang, F., Fan, X., 2017. Utilization of

MoS_2 and graphene to enhance the photocatalytic activity of Cu_2O for oxidative CC bond formation. Appl. Catal. B Environ. 213, 1–8.

Fan, W., Yu, X., Lu, H.-C., Bai, H., Zhang, C., Shi, W., 2016. Fabrication of TiO_2/RGO/Cu_2O heterostructure for photoelectrochemical hydrogen production. Appl. Catal. B Environ. 181, 7–15.

Hardcastle, F., 2011. Raman spectroscopy of titania (TiO_2) nanotubular water-splitting catalysts. J. Acad Market. Sci. 65, 43–48.

Prabhakaran, G., Murugan, R., 2014. Synthesis of Cu_2O nanospheres and cubes: their structural, optical and magnetic properties. Adv. Mat. Res. 114–117.

Ohsaka, T., Izumi, F., Fujiki, Y., 1978. Raman spectrum of anatase, TiO_2, J. Raman. Spectrosc. 7, 321–324.

Cherstiouk, O.V., Simonov, P.A., Oshchepkov, A.G., Zaikovskii, V.I., Kardash, T.Y., Bonnefont, A., Parmon, V.N., Savinova, E.R., 2016. Electrocatalysis of the hydrogen oxidation reaction on carbon-supported bimetallic NiCu particles prepared by an improved wet chemical synthesis. J. Electroanal. Chem. 783, 146–151.

Gupta, A., Arunachalam, V., Vasudevan, S., 2015. Water dispersible, positively and negatively charged MoS_2 nanosheets: surface chemistry and the role of surfactant binding. J. Phys. Chem. Lett. 6, 739–744.

Bao, C., Guo, Y., Song, L., Kan, Y., Qian, X., Hu, Y., 2011. In situ preparation of functionalized graphene oxide/epoxy nanocomposites with effective reinforcements. J. Mater. Chem. 21, 13290–13298.

Yuan, B., Sun, Y., Chen, X., Shi, Y., Dai, H., He, S., 2018a. Poorly-/well-dispersed graphene: abnormal influence on flammability and fire behavior of intumescent flame retardant. Compos. Part A 109, 345–354.

Huang, K.-J., Wang, L., Liu, Y.-J., Wang, H.-B., Liu, Y.-M., Wang, L.-L., 2013. Synthesis of polyaniline/2-dimensional graphene analog MoS_2 composites for high-performance supercapacitor. Electrochim. Acta 109, 587–594.

Yuan, Y., Yu, B., Shi, Y., Ma, C., Song, L., Hu, W., Hu, Y., 2018b. Highly efficient catalysts for reducing toxic gases generation change with temperature of rigid polyurethane foam nanocomposites: a comparative investigation. Compos. Part A 112, 142–154.

Wang, B., Sheng, H., Shi, Y., Song, L., Zhang, Y., Hu, Y., Hu, W., 2016. The influence of zinc hydroxystannate on reducing toxic gases (CO, NOx and HCN) generation and fire hazards of thermoplastic polyurethane composites. J. Hazard. Mater. 314, 260–269.

Thirumal, M., Khastgir, D., Singha, N.K., Manjunath, B., Naik, Y., 2007. Mechanical, morphological and thermal properties of rigid polyurethane foam: effect of the fillers. Cell. Polym. 26, 245.

Camino, G., Costa, L., Trossarelli, L., 1984. Study of the mechanism of intumescence in fire retardant polymers: part I—thermal degradation of ammonium polyphosphate-pentaerythritol mixtures. Polym. Degrad. Stab. 6, 243–252.

Modesti, M., Lorenzetti, A., Besco, S., Hrelja, D., Semenzato, S., Bertani, R., Michelin, R., 2008. Synergism between flame retardant and modified layered silicate on thermal stability and fire behaviour of polyurethane nanocomposite foams. Polym. Degrad. Stab. 93, 2166–2171.

Bissessur, R., Kanatzidis, M.G., Schindler, J., Kannewurf, C., 1993. Encapsulation of polymers into MoS_2 and metal to insulator transition in metastable MoS_2, Journal of the Chemical Society. Chem. Commun. 1582–1585.

Cao, Y., Feng, J., Wu, P., 2010. Preparation of organically dispersible graphene nanosheet powders through a lyophilization method and their poly (lactic acid) composites. Carbon 48, 3834–3839.

Wang, X., Xing, W., Feng, X., Yu, B., Lu, H., Song, L., Hu, Y., 2014b. The effect of metal oxide decorated graphene hybrids on the improved thermal stability and the reduced smoke toxicity in epoxy resins. Chem. Eng. J. 250, 214–221.

Laachachi, A., Cochez, M., Leroy, E., Ferriol, M., Lopez-Cuesta, J., 2007. Fire retardant systems in poly (methyl methacrylate): interactions between metal oxide nanoparticles and phosphinates. Polym. Degrad. Stab. 92, 61–69.

Laachachi, A., Cochez, M., Ferriol, M., Lopez-Cuesta, J., Leroy, E., 2005. Influence of TiO_2 and Fe_2O_3 fillers on the thermal properties of poly (methyl methacrylate)(PMMA). Mater. Lett. 59, 36–39.

Shi, Y., Yu, B., Zhou, K., Yuen, R.K., Gui, Z., Hu, Y., Jiang, S., 2015. Novel $CuCo_2O_4$/graphitic carbon nitride nanohybrids: highly effective catalysts for reducing CO generation and fire hazards of thermoplastic polyurethane nanocomposites. J. Hazard. Mater. 293, 87–96.

Stec, A.A., Hull, T.R., 2011. Assessment of the fire toxicity of building insulation materials. Energ Buildings. 43, 498–506.

Liu, X., Hao, J., Gaan, S., 2016. Recent studies on the decomposition and strategies of smoke and toxicity suppression for polyurethane based materials. RSC Adv. 6, 74742–74756.

Fang, M., Wang, K., Lu, H., Yang, Y., Nutt, S., 2010. Single-layer graphene nanosheets with controlled grafting of polymer chains. J. Mater. Chem. 20, 1982–1992.

Bian, X.C., Tang, J.H., Li, Z.M., 2008. Flame retardancy of hollow glass microsphere/rigid polyurethane foams in the presence of expandable graphite. J. Appl. Polym. Sci. 109, 1935–1943.

Ye, L., Meng, X.-Y., Ji, X., Li, Z.-M., Tang, J.-H., 2009. Synthesis and characterization of expandable graphite–poly (methyl methacrylate) composite particles and their application to flame retardation of rigid polyurethane foams. Polym. Degrad. Stab. 94, 971–979.

Meng, X.Y., Ye, L., Zhang, X.G., Tang, P.M., Tang, J.H., Ji, X., Li, Z.M., 2009. Effects of expandable graphite and ammonium polyphosphate on the flame-retardant and mechanical properties of rigid polyurethane foams. J. Appl. Polym. Sci. 114, 853–863.

Xing, W., Yuan, H., Yang, H., Song, L., Hu, Y., 2013. Functionalized lignin for halogen-free flame retardant rigid polyurethane foam: preparation, thermal stability, fire performance and mechanical properties. J. Polym. Res. 20, 234.

Yan, D., Xu, L., Chen, C., Tang, J., Ji, X., Li, Z., 2012. Enhanced mechanical and thermal properties of rigid polyurethane foam composites containing graphene nanosheets and carbon nanotubes. Polym. Int. 61, 1107–1114.